Published in final edited form as:

Nature. 2009 January 8; 457(7226): 191–195. doi:10.1038/nature07591.

MYELOMONOCYTIC CELL RECRUITMENT CAUSES FATAL CNS VASCULAR INJURY DURING ACUTE VIRAL MENINGITIS

Jiyun V. Kim[1,3], **Silvia S. Kang**[2,3], **Michael L. Dustin**[1], and **Dorian B. McGavern**[2]

[1]Program in Molecular Pathogenesis, Helen L. and Martin S. Kimmel Center for Biology and Medicine, Skirball Institute of Biomolecular Medicine, New York University School of Medicine, New York, New York 10016, USA

[2]Department of Immunology and Microbial Sciences, The Scripps Research Institute, La Jolla, California 92037, USA

Lymphocytic choriomeningitis virus (LCMV) 1 infection of the murine brain elicits fatal immunopathology through blood brain barrier (BBB) breakdown 2 and convulsive seizures 3. While LCMV-specific cytotoxic T lymphocytes (CTL) are essential for disease 4, their mechanism of action is not known. To gain novel insights into disease pathogenesis, we visualized the dynamics of immune cells in the meninges by two-photon microscopy (TPM). We observed motile CTL and massive secondary recruitment of pathogenic monocytes and neutrophils that were required for vascular leakage and acute lethality. CTL expressed multiple chemoattractants capable of recruiting myelomonocytic cells. We conclude that a $CD8^+$ T cell dependent disorder can proceed in the absence of direct T cell effector mechanisms and rely instead on CTL recruited myelomonocytic cells.

To examine the dynamics of LCMV-specific CTL, we transferred 1×10^5 naïve GFP-tagged $D^bGP_{33–41}$ T cell receptor (TCR) transgenic (tg) $CD8^+$ T cells (GFP^+ P14 cells) into B6 mice one day prior to intracranial (i.c.) inoculation with LCMV Armstrong (Arm). TPM was performed through a thinned skull window to visualize the meninges overlying the visual cortex in asymptomatic (day 5) and symptomatic (day 6) mice (Fig. 1; Movie 1). In contrast to the few P14 cells observed on day 5 (Fig. 1a), the number of GFP^+ P14 cells was dramatically increased in the meninges and perivascular regions on day 6 (Fig. 1b, c). To determine if GFP^+ P14 cells were engaging in antigen specific interactions, we analyzed their motion in the presence of control antibody (IgG) or a blocking monoclonal antibody to D^b (anti-class I) introduced into the subarachnoid space through a small craniotomy (Fig. 1d-i). P14 speed averaged 3.41 ± 0.27 μm/min (mean ± s.e.m.) in the absence of the craniotomy and 3.04 ± 0.33 μm/min in the presence of the craniotomy and IgG (Fig. 1j). The anti-class I significantly increased the speed of P14 cells to 5.16 ± 0.46 μm/min (Fig. 1j,k) and decreased the arrest coefficient (Fig. 1l), but did not influence the speed of CTL specific for an irrelevant antigen (Fig. S1). This significant change in P14 cell speed and arrest

Correspondence and requests for materials should be addressed to M.L.D. (Email: dustin@saturn.med.nyu.edu) and D.B.M. (Email: mcgad@scripps.edu).

[3]These authors contributed equally to this work.

following anti-class I treatment was observed in all mice examined and did not depend on CTL abundance (Fig. S2). GFP^+ P14 CTL migration appeared random (Fig. S3), with confined motion at longer times that was reversed by anti-class I. Comparison of the speed distributions showed that the entire population shifts following anti-class I treatment (Fig. 1k), suggesting that all GFP^+ P14 cells encountered antigen. Despite this high frequency of antigen encounter, CTL rarely synapsed with any one target for > 10 minutes (Fig. 1g,m). These intravital observations raised questions about the infected target population and the CTL effector mechanisms utilized during fatal meningitis.

We identified the LCMV infected cells through immunohistochemical studies (Fig. 2 & S4; Movie 2). The main LCMV infected population in the meninges and around meningeal vasculature was ER-$TR7^+$ stromal cells. LCMV infection was occasionally observed in $CD45^+$ infiltrating leukocytes and astrocytic foot processes that comprise the glial limitans (Fig. S4). Infection of endothelium and smooth muscle cells / pericytes was never observed (Fig. S4). ER-$TR7^+$ stromal cells support rapid migration of $CD8^+$ and $CD4^+$ T cells in lymph nodes 5 and may provide strong chemokinetic signals that can overwhelm synapse forming stop signals 6. This might explain the paucity of antigen specific arrest (Fig. 1).

Since $CD8^+$ T cells are essential for pathology 4, we evaluated several CTL effector mechanisms using genetic knockout and mutant mice (Fig. 3a). Surprisingly, mice with single deficiencies in all major CTL effector pathways – IFNγ receptor, TNFα, Fas, granzymes, perforin (PFP), and the degranulation pathway (*Jinx* mutant) -succumbed to the convulsive seizures observed following LCMV infection of wild type mice. The delay in disease onset observed in perforin knockout mice was recently attributed to slower CTL recruitment into CNS 7. These data supported the imaging studies in suggesting that CTL effector functions might not be responsible for rapid onset disease.

To investigate other effectors, we temporally examined the composition of the CNS infiltrate following i.c. LCMV infection (Fig. 3b & S5). Baseline populations prevailed until day 6 at which point monocytes / macrophages were massively recruited into the CNS. A low number of these cells preceded the arrival of CTL by 2 days. At day 6 a small increase in the numbers of neutrophils, $CD4^+$ T cells, and B cells was also observed; however, the latter two populations are not required for disease 8,9. It should be noted that our methodology accounts primarily for extravasated leukocytes, as cells arrested in the vasculature (e.g., neutrophils) are expunged during intracardiac saline perfusions. Nevertheless, our results demonstrate a minimal innate cellular response to the virus alone and massive recruitment of myelomonocytic cells that coincided with the arrival of CTL at day 6.

We next asked whether monocytes and/or neutrophils were required for the seizure-induced death on day 6 (Fig. 3c–f). Neutrophil depletion with low dose anti-Gr-1 antibody 10 (Fig. 3c–d) or monocyte infiltration blockade using CCR2 deficient mice 11 (Fig. 3e–f) had no effect on the nature or kinetics of death. Therefore, we hypothesized that both populations might have the potential to induce CNS injury. To test this hypothesis, we depleted monocytes and neutrophils simultaneously by administering high dose anti-Gr-1 to CCR2 knockout mice (Fig. 3e,f). When both cell populations were depleted, seizure-induced death

at day 6 was averted and survival was extended by 3 days (Fig. 3e,f), despite a normal frequency of virus-specific CTL on day 6 (data not shown). These data suggested that myelomonocytic cells were highly pathogenic and were responsible for the rapid onset seizure-induced death observed at day 6.

During TPM analyses of GFP^+ P14 cells, we often noted that the vasculature appeared ragged and displayed plasma leakage tracked with intravascular injected quantum dots (Movie 3). We considered that the seizure-induced death at day 6 might be induced by vascular leakage caused by myelomonocytic cells. To test this possibility, we conducted TPM in LCMV infected LysM-GFP mice, in which neutrophils and monocytes are labeled with GFP, to detect the relationship between myelomonocytic extravasation and vascular leakage. There was a tight correspondence between locally synchronized LysM-GFP^+ cell extravasation and vascular leakage on day 6 (Fig. 4e–h; Movie 4).

To determine the relative contribution of neutrophils versus monocytes to vascular injury, we imaged LysM-GFP mice injected with low dose anti-Gr-1 antibody, which depletes only neutrophils (Fig. 3c & S6). Interestingly, synchronous extravasation of LysM-GFP^+ cells was not observed in low dose Gr-1-depleted mice (Fig. 4i–l; Movie 5), suggesting that synchronously extravasating LysM-GFP^+ cells are neutrophils. In neutrophil depleted LysM-GFP mice, we observed perivascular LysM-GFP+ cells (i.e., monocytes / macrophages) in areas of transient vascular leakage. Unlike neutrophils that display intravascular accumulation followed by explosive extravasation with vascular leakage, the monocytes accumulated more gradually in vascular sites that nonetheless displayed leakage. Statistically, sustained vascular leakage was only correlated ($r = 0.99$; $p < 0.0001$) with neutrophils (Fig. 4m). The presence of intra- or extravascular P14 CTL was not associated with either pattern of vascular leakage (Fig. 4o). Quantum dot leakage was not observed on day 5 post-infection (Fig. 4p) despite low numbers of infiltrating monocytes (Fig. 3b). Vascular injury occurred only at day 6 post-infection and extended into the brain parenchyma (Fig. 4q). Myelomonocytic cells were restricted to the meninges on day 6 (Fig. 4q,r & S10).

The impact of myelomonocytic cells on vascular injury was further assessed by quantifying leakage of Evans blue dye into the brain (Fig. S7). Only mice depleted of both monocytes and neutrophils showed significant preservation of vascular integrity at day 6 post-infection (Fig. S7e,f). Depletion of monocytes (Fig. S7d,f) or neutrophils (Fig. S7c,f) alone failed to prevent Evans blue leakage. Interestingly, in untreated wild type mice at day 6 post-infection, we observed substantial leakage of Evans blue from meningeal blood vessels into the brain parenchyma (Fig. S8), reflecting disrupted BBB integrity, which has the potential to cause severe seizures 12.

To examine a potential mechanism by which CTL attract myelomonocytic cells, we used gene arrays to quantify differentially regulated transcripts in the brains of mock-versus d6 LCMV-infected mice. Our results revealed a statistically significant increase ($p < 0.05$) in 6 chemokines (CCL2 - 7.3 fold, CCL3 – 8.1 fold, CCL4 – 1.6 fold, CCL5 – 5.6 fold, CCL7 – 4.2 fold, CXCL2 – 2.8 fold) and 2 chemokine receptors (CCR1 – 2.6 fold, CCR2 – 3.6 fold) that can recruit myelomonocytic cells into the CNS. Because it was reported that none of

these chemokines were observed in the CNS of T cell-deficient mice infected i.c. with LCMV 13, we next used flow cytometry to examine which of these chemokines were produced by virus-specific P14 cells (Fig. S9). Our flow cytometric analyses of CNS and splenic P14 CTL at day 6 revealed that CCL3, CCL4, and CCL5 were all produced at the protein level, which was confirmed using gene arrays 14,15. Both CCL3 and CCL4 required $GP_{33–41}$ peptide stimulation for maximum synthesis, whereas CCL5 was produced upon differentiation from naïve to effector cells and was not further upregulated upon peptide stimulation.

It is well known that $CD8^+$ T cells are required for LCMV-induced meningitis 4 and vascular leakage 16. Our results revealed that P14 CTL could produce three of the chemokines responsible for attracting the myelomonocytic cells responsible for vascular injury (Fig. 4 & S7) and rapid onset seizure-induced death (Fig. 3). To establish a direct link between $CD8^+$ T cells and CNS myelomonocytic cell recruitment, we infected mice with LCMV and administered anti-CD8 antibody at days 4 and 5 post-infection – after CTL priming. This treatment, which reduced the number of $CD8^+$ T cells in the CNS by 94%, prevented the rapid onset of seizures at day 6 post-infection (data not shown), and significantly reduced the number of monocytes and neutrophils in the CNS (Fig. S10). These data indicate that virus-specific CTL can contribute to the recruitment of pathogenic myelomonocytic cells either by directly releasing chemoattractants or possibly by inducing other cells to release chemoattractants.

The requirement for $CD8^+$ T cells in the pathogenesis of LCMV meningitis led to the proposal that CTL were directly responsible for tissue injury and death 17. We propose that CTL activation through transient interactions with infected cells leads to massive recruitment of myelomonocytic cells, which compromise vascular integrity and initiate fatal convulsive seizures 3. It is likely that once seizure-induced death is averted, infected mice ultimately succumb to another pathogenic mechanism possibly mediated by CTL 18.

It is well established that neutrophil extravasation can be linked to vascular leakage 19–21, and this process usually depends on signaling between leukocytes and endothelial cells 22. Neutrophil extravasation causes tissue injury in many models including reperfusion injury and sepsis 23,24. Using TPM we directly visualized this classical process in LCMV meningitis. Monocytes have been associated with atherosclerosis 25 and facilitating the trafficking of neutrophils 26. Our results suggest that monocytes also contribute vascular leakage, possibly through a mechanism linked to adherence to the blood vessels 27 and / or chemokine release 28. Recognizing the complementary pathogenic functions of neutrophils and monocytes is critical for devising therapeutic approaches in $CD8^+$ T cell-mediated pathology.

It is not clear why $CD8^+$ T cells recruit myelomonocytic cells to a site of viral infection. $CD4^+$ Th17 cells produce IL-17 to coordinate neutrophil recruitment, but anti-viral $CD8^+$ T cells express transcription factors that suppress this program 29, and we observed no IL-17 production by peptide-stimulated P14 cells (data not shown). Therapies directed at reducing myelomonocytic activation are obvious treatment candidates to prevent the mode of immunopathology we observed, but are challenging due to their numerous effector

mechanisms, fast turnover, and acute importance in host defense. A more tractable approach might be to target the chemotactic mechanisms used by CTL to attract myelomonocytic cells, or, alternatively, to enhance CTL-mediated killing of relevant targets by improving immunological synapse formation or stability 30. The latter approach might break the feedback to the pathogenic myelomonocytic arm and improve survival as well as immunity in viral infections of the CNS.

METHODS SUMMARY

To induce meningitis, mice were infected intracerebrally with the Armstrong strain of LCMV. Fluorescent protein tagged virus specific P14 CTL and myelomonocytic cells were imaged through a surgically thinned skull using a Bio-Rad multi-photon microscope. Skull was detected using second harmonic signal, and meningeal vasculature was visualized by intravenously injecting quantum dots 10 minutes prior imaging. All imaging data were processed and analyzed using Volocity software.

For flow cytometric studies, mice received an intracardiac perfusion with saline. The CNS was then harvested, treated with collagenase D, and mononuclear cells were isolated using a Percoll gradient. Afterward, mononuclear cells were treated with Fc block, serum, stained with fluorescently labeled antibodies, and acquired using a Becton Dickinson digital flow cytometer. Data were analyzed using the FlowJo software.

Myelomonocytic cells were depleted from mice by intraperitoneally injecting 125 ug (low dose) or 400 ug (high dose) of purified, endotoxin free anti-Gr-1 (RB6-8C5 clone). Low dose antibody was injected once at day 4 post-infection to deplete neutrophils only, whereas high dose antibody (to deplete both neutrophils and monocytes) was injected daily starting at day 3 post-infection. $CD8^+$ T cells were depleted by injecting 1000 ug of purified, endotoxin free anti-CD8 (53-6.72 clone) on day 4 and 500 ug day 5 post-LCMV infection.

CNS vascular leakage was evaluated by retroorbitally injecting mice with Evans Blue. After 4 hours, mice were perfused with saline and brains were harvested. Evans blue was extracted using N,N-dimethyl formamide and quantified using a Varioskan Flash fluorometer (620nm excitation; 695 nm emission). Representative qualitative images of Evans Blue permeability from were photographed using a digital camera, and fluorescence images on vibratome brain sections were captured using a BioRad MRC2100 confocal microscope (637 nm excitation).

All immunohistochemistry was performed on 6-μm frozen sections or 100-μm vibratome sections. Primary antibodies were detected with fluorescently labeled secondary reagents and visualized using an Axiovert S100 immunofluorescence microscope or a BioRad MRC2100 confocal microscope.

To quantify gene expression changes in the LCMV-infected CNS, total RNA was isolated from saline perfused mock- and d6 LCMV infected brains and hybridized overnight to the Mouse Exon 1.0 ST Array. Chips were scanned using the Affymetrix GeneChip Scanner. The analysis was run using XRAY (version 2.3) software - the Excel add-in from Biotique Systems Inc. Myelomonocytic cell chemoattractants with increased expression at day 6 post-

infection were identified, and their expression at the protein level by P14 CTL was quantified flow cytometrically.

METHODS

Transgenic mice

C57BL/6 (B6), B6 GFP$^+$D^{b}GP$_{33–41}$ TCR-tg (GFP$^+$ P14) 31, B6 Thy1.1$^+$D^{b}GP$_{33–41}$ TCR-tg (Thy1.1$^+$ P14), B6 OT-I TCR-tg, B6 Perforin$^{-/-}$ (PFP$^{-/-}$), B6 TNFα$^{-/-}$, and B6 IFNγR$^{-/-}$ mice were bred and maintained in a closed breeding facility at The Scripps Research Institute. B6, B6 CCR2$^{-/-}$ and B6 Fas$^{-/-}$ mice were obtained from The Jackson Laboratories. The following mice were generous gifts from other investigators: B6 LysM-GFP heterozygous knock in mice (LysM $^{gfp/+}$) (Dr. Thomas Graf; Albert Einstein) 32, B6 *Jinx* mice (Dr. Bruce Beutler; The Scripps Research Institute) 33, and 129 granzyme a × b cluster knockout mice (deficient in granzymes a, b, c, and f) (Dr. Timothy Ley; Washington University) 34. All mice were housed in specific pathogen-free conditions and treated in accordance with Institutional Animal Care and Use Committee protocols of The Scripps Research Institute and New York University School of Medicine.

Virus

To induce meningitis, adult mice at 6–8 week of age were infected intracerebrally (i.c.) with 1×10^3 plaque forming units (PFU) of LCMV Armstrong (Arm) clone 53b. Survival was monitored daily. Stocks were prepared by a single passage on BHK-21 cells, and viral titers were determined by plaque formation on Vero cells.

Mononuclear cell isolations and tissue processing

To obtain cell suspensions for flow cytometric analysis, the brain and spinal cord were harvested from mice after an intracardiac perfusion with 25 ml of 0.9% saline solution to remove the contaminating blood lymphocytes. The CNS was then incubated with 1 ml collagenase D (1 mg/ml; Roche) at 37°C for 30 minutes. Single-cell suspensions were prepared by mechanical disruption through a 100-μm filter. Brain-infiltrating leukocytes were isolated and counted as described previously 35. For immunohistochemical analyses, fresh, unfixed brain tissue was either frozen on dry ice in optimal cutting temperature (OCT; Tissue-Tek) (for frozen sectioning) or incubated overnight with 4% PFA (for vibratome sectioning).

GFP$^+$P14 Cell Transfer

CD8$^+$ T cells were purified from GFP$^+$ P14 mouse splenocytes by negative selection (Stem Cell Technologies). The purity after enrichment was determined to be greater than 98%. For imaging studies, 1×10^5 purified GFP$^+$ P14 CD8$^+$ T cells were injected i.v. into naïve mice. One day later the mice were challenged i.c. with LCMV Arm.

OT-I Cell Transfer

Splenocyes were isolated from OT-I mice and expanded *in vitro* for 7 days in RPMI 1640 containing 10% FBS, 1% L-glutamine, 1% penicillin/streptomycin, 500 units/ml IL-2, and 1

μg/mL $OVA_{257–264}$ (SIINFEKL) peptide. The cells were then labeled with 5 μM CFSE in PBS (InVitrogen) at 37°C for 5 min and washed 3 times in PBS. $1×10^7$ CFSE-labeled OT-I cells were transferred into each d6 LCMV-infected B6 mouse and intravital imaging was performed 6–12 hrs after the transfer.

CD8 T cell Depletion

To deplete $CD8^+$ T cells from LCMV infected B6 mice, 1000 ug of purified, endotoxin free anti-CD8 (53-6.72 clone) was injected on day 4 and 500 ug was injected on day 5 post-LCMV infection. This resulted in a 94% reduction in CNS-infiltrating $CD8^+$ T cells. The control group for these experiments was injected with polyclonal rat IgG (Jackson ImmunoResearch Laboratories).

Neutrophil Depletion

To deplete myelomonocytic cells from B6 and B6 $CCR2^{-/-}$ mice, 125 ug (low dose) or 400 ug (high dose) of purified, endotoxin free anti-Gr-1 (RB6-8C5 clone) antibody was injected i.p. The RB6-85C hybridoma was generously provided by Dr. Paul Allen (Washington University). Low dose antibody was injected once at day 4 post-infection to deplete neutrophils only. This resulted in an 87% reduction of neutrophils in the CNS and 98% reduction in the blood. High dose antibody was injected daily starting at day 3 post-infection to deplete both neutrophils and monocytes. Injection of polyclonal rat IgG (Jackson ImmunoResearch Laboratories) was used as a control.

Gene Array

Total RNA from mock and d6 LCMV infected brains (n=3 mice per group) was isolated using a using a Qiagen RNeasy Midi prep kit and then quantified using Nanodrop ND-1000. Sample quality was checked using Agilent 2100 Bioanalyzer. In order to remove most of the ribosomal RNA from the RNA, 2.5ug of each sample was taken through RiboMinus (Invitrogen). After RiboMinus treatment samples were amplified and labeled using the GeneChip Whole Transcript Sense Target Labeling Assay (Affymetrix). Samples were checked by gel shift assay to assess labeling efficiency as described in the GeneChip Whole Transcript Sense Target Labeling Assay Manual. Samples were hybridized overnight to the Mouse Exon 1.0 ST Array. Hybridization and scanning of samples to arrays was performed using standard Affymetrix protocols and reagents from the GeneChip Hybridization, Wash, and Stain Kit. Chips were scanned using the Affymetrix GeneChip Scanner 3000 7G with default settings and a target intensity of 250 for scaling. In order to identify genes with differential gene expression or alternative splicing between the two groups, we studied 3 hybridizations each on the Mouse Exon 1.0 ST array using mixed model analysis of variance. The analysis was run using XRAY (version 2.3) software - the Excel add-in from Biotique Systems Inc.

Analysis of BBB integrity

To quantify BBB permeability, Evans blue leakage in the brains of mock infected or LCMV i.c. infected mice was assessed. On the indicated day, mice were injected retroorbitally with 20 mg per kg Evans Blue (Sigma). After 4 hours, the brains were extracted after a PBS

perfusion, which was used to eliminate circulating Evans Blue. The tissue was homogenized in 600μl of N,N-dimethyl formamide (Sigma). The homogenate was transferred to new tubes, centrifuged at 14,000 rpm for 20 mins at 4°C and the supernatant was plated in triplicate wells in a 96 well flat bottom plate. For quantification an Evans Blue standard was diluted in the supernatant of a PBS-perfused uninfected brain that received no Evans Blue, but was homogenized in N,N-dimethyl formamide. All samples plated in triplicate were read using a Varioskan Flash fluorometer (620nm excitation; 695 nm emission) (Thermo Scientific). The excitation and emission wavelengths were determined by spectral scanning to be optimal for Evans blue. Representative qualitative images of Evans Blue permeability from PBS perfused brains were taken using a digital camera.

Flow Cytometry

Brain-infiltrating leukocytes were harvested and blocked with 3.3 μg/ml anti-mouse CD16/CD32 (Fc Block; BD Biosciences) in PBS containing 1% FBS and 0.1% sodium azide for 15 minutes on ice. After Fc block, cells were stained with the following conjugated antibodies: CD45.2 FITC (104), Thy1.2 PE (53-2.1), CD19 PerCP CY5.5 (1D3), Gr1 APC (RB6-8C5), CD4 APC Cy7 (GK1.5) (BD Biosciences), CD8 Pacific Blue (Caltag), MCA771 PE (7/4; Serotec), and anti-CD11b PE/Cy7 (M1/70; ebioscience). Cells were acquired using a digital flow cytometer (Digital LSR II; Becton Dickinson) and flow cytometric data were analyzed with FlowJo software (Tree Star, Inc).

Intracellular chemokine staining

Mice seeded with 10^4 P14 Thy1.1 cells on day -1 were infected with 10^3 PFU LCMV Arm i.c. on day 0. On day 6 post infection, brain-infiltrating leukocytes and splenocytes from infected mice and splenocytes from naïve P14 Thy1.1 mice were harvested and stimulated with 50U/ml IL-2 (Roche), 1ug/ml Brefeldin A (Sigma-Aldrich) and 1ug/ml $GP_{33–41}$ peptide for 5 hours at 37°C. Cells were centrifuged and then blocked with 3.3 μg/ml anti-mouse CD16/CD32 (Fc Block; BD Biosciences) in PBS containing 1% FBS and 0.1% sodium azide for 15 minutes on ice. After Fc block, cells were stained with the following conjugated antibodies: CD45.2 FITC (104), Thy1.1 PerCP (53-2.1) (BD Biosciences) and CD8 APC/Cy7 (53-6.7) (Biolegend) for 30 minutes on ice. Cells were washed and fixed for 10 minutes at RT in PBS containing 1% FBS, 0.1% sodium azide, 1% PFA and 0.1% saponin. Intracellular staining and washes for all intracellular steps were conducted in PBS containing 1% FBS, 0.1% sodium azide and 0.1% saponin. Cells were stained with PE conjugated antibodies against CCL-2 (1:100, Biolegend) and CCL3 (1:100, R&D systems), biotinylated antibodies against CCL5, CXCL2 (1:100, R&D systems) or purified antibodies against CCL4 (1:200, BD Bioscience) and CCL7 (1:100, R&D systems) for 30 minutes on ice. Secondary and tertiary incubations with biotinylated anti-rat IgG1 (1:100, Biolegend), PE conjugated donkey anti-goat (1:100, Jackson Immunoresearch Laboratories) or SA-APC (1:100 Invitrogen) were used in subsequent steps. After the final wash, cells were resuspended in PBS containing in 1% FBS and 0.1% sodium azide and acquired using a digital flow cytometer.

Immunohistochemistry

To examine LCMV localization, 6-μm frozen sections were cut, fixed with 4% paraformaldehyde (PFA) for 15 min, blocked with an avidin/biotin-blocking kit (Vector Laboratories), and stained for 1 h at room temperature with primary guinea pig antibodies against LCMV (1:500). Secondary and tertiary incubations with biotinylated donkey anti-guinea pig (1:200; Jackson ImmunoResearch Laboratories) and streptavidin Rhod-X (1:250; Jackson ImmunoResearch Laboratories), respectively, were done to detect LCMV antigen. Co-labeling of fibroblasts (anti-ER-TR7; 1:100; Abcam), astrocytes (anti-GFAP; 1:800, DakoCytomation), infiltrates (anti-CD45.2; 1:100, BD Biosciences), endothelium (anti-CD31; 1:200; Chemicon) or smooth muscle actin (anti-SMA; 1:100; Abcam) was also conducted in conjunction with anti-LCMV staining. The cell marker specific antibodies were detected with secondaries conjugated to FITC (1:200; Jackson ImmunoResearch Laboratories). All working stocks of primary and secondary reagents were diluted in PBS containing 2% fetal bovine serum (FBS). To generate 3D renderings of LCMV-infected fibroblasts, 100-μm vibratome sections were cut using a Leica VT1000S (Leica) and blocked with PBS containing 10% FBS and 0.1% saponin for 1 h at room temperature. Staining for LCMV and fibroblasts was conducted as indicated above, with the exception that the antibodies were diluted in PBS containing 2% FBS supplemented with 0.1% saponin. To obtain images of Evans Blue leakage, 100-μm vibratome sections from PBS perfused mice injected with Evans Blue (as described above) were stained with anti-CD31 (1:200; Chemicon) diluted in PBS containing 2% FBS supplemented with 0.5% triton-x (Sigma-Aldrich). CD31 was detected and amplified with a FITC conjugated goat anti-hamster antibody (1:200; Jackson ImmunoResearch Laboratories), a rabbit anti-FITC antibody (1:200; Zymed) and a FITC conjugated anti-rabbit antibody (1:200; Jackson ImmunoResearch Laboratories). All sections described above were further stained with 1 μg/ml DAPI (Sigma-Aldrich) for 3 minutes at room temperature to visualize cell nuclei.

One-photon microscopy

2D co-localization images to determine whether LCMV infected fibroblasts, leukocytes, astrocytes, endothelium, or smooth muscle cells / pericytes (Fig. 2 & S3) were captured from 6-μm frozen using a MRC2100 confocal microscope (Bio-Rad Laboratories) fitted with 40x, 63x, and 100x oil objectives and seven laser lines that excite at 405nm, 457nm, 477nm, 488nm, 514nm, 543nm, and 637nm (Carl Zeiss MicroImaging, Inc). 3D *z*-stacks were captured with from 100-μm vibratome sections using a step size of 0.1 μm. Maximal projections and 3D reconstructions (Fig. 2) were generated using Volocity software (Improvision).

Intravital two-photon microscopy

Mice were anaesthetized and maintained at core temp of 37°C. Thinned skull and open skull surgery were performed and imaged using Bio-Rad Radiance multi-photon microscope (Zeiss, Thornwood, NY) powered by Tsunami pulsed laser (Spectraphysics) tuned to 920 nm as described previously 36. Bone (second harmonic signal), GFP-labeled cells (GFP P14 or LysM-GFP), and intravascular quantum dots (Qdots) were visualized using band-pass filters 400/10, 480/30 and 540/30, respectively. To visualize meningeal vasculature, mice

were injected i.v. 10 min prior to imaging with 50 μl Qtracker 655nm non-targeted quantum dots (0.2 uM) (Invitrogen). For MHC I blocking studies, H-2D^b monoclonal antibody and isotype control (10 μg/ml) in 200 μl of artificial cerebral spinal fluid (119 mM NaCl, 26.2 mM $NaHCO_3$, 2.5 mm KCl, 1 mM NaH_2PO_4, 1.3 mM $MgCl_2$, 1.2 mM $CaCl_2$, 0.4 % glucose, pH 7.4) were administered through a partial open skull adjacent to the thinned skull viewing area. Antibodies were incubated for 15–30 min to permit adequate local tissue diffusion. CTL dynamics were imaged through the adjacent thinned skull. For all imaging studies, stacks of images were acquired using step sizes of 1–3 μm to a depth of 200 μm below the skull using 20x, 40x or 60x water dipping objectives. Time-lapse movies were acquired with 1- to 1.5-min intervals between 3D stacks. Image analysis was performed and cell movements were tracked using Volocity software and graphs were determined using Graph Prism4. The average speed (μm/min) of CTL and myelomonocytic cells was quantified manually from 30 min time lapses with 20 intervals. Arrest duration (min) is the total time that a CTL slowed to < 2 μm/min interval / instantaneous speed during a 30 min time lapse. The arrest coefficient is the percentage of total elapsed time that CTL spent moving < 2 μm/min. The confinement index was calculated by dividing the displacement (or distance a cell traveled) by the speed. The motility coefficient was calculated as (mean displacement)^2 / (4 × time). Histograms showing the relative frequency of CTL velocities under different conditions were generated using a bin size of 2 μm/min and Gaussian curve fitting. The fluorescence ratio (FR) of extravascular (ev) to intravascular (iv) Qdot and GFP signal was calculated by first quantifying the mean fluorescence intensity in defined extra- and intravascular regions. Mean extravascular fluorescence was then divided by mean intravascular fluorescence for each channel (FR ev/iv) and normalized to the ratio at time 0 (FR_{t0}) by division ($FRev/iv / FR_{t0}$). All imaging data are representative of at least three independent experiments.

Sagittal Brain Reconstructions

Two-color organ reconstructions to visualize the distribution of LysM-GFP$^+$ cells on 6-μm frozen sections (Fig. S10) were obtained using an immunofluorescence microscope (Axiovert S100; Carl Zeiss MicroImaging, Inc.) fitted with an automated *xy* stage, a color digital camera (Axiocam, Carl Zeiss MicroImaging, Inc.), and a 5× objective. Registered images were captured for each field on the tissue section, and reconstructions were performed using the MosaiX function in KS300 image analysis software (Carl Zeiss MicroImaging, Inc.).

Statistical Analysis

Statistical significance ($p < 0.05$) was determined using a Student's *t* test, a Mann-Whitney rank sum test for populations with non-Gaussian distributions, or a one way ANOVA for experiments containing more than two groups. Correlations were evaluated using a Pearson Product Moment Correlation test.

Supplementary Material

Refer to Web version on PubMed Central for supplementary material.

ACKNOWLEDGMENTS

This work was supported by National Institutes of Health grants AI070967-01 (D.B.M.), AI055037 (M.L.D.), a grant from The Burroughs Wellcome Fund (D.B.M.), and the Dana Foundation (M.L.D.). S.S.K. was supported by a National Institutes of Health training grant NS041219-06 and is presently supported by a National Research Service Award (NS061447-01), and J.V.K. is supported by a Multiple Sclerosis Society Center Grant (PI -J. Salzer). We would like to thank Christopher Yau for excellent technical support and the Scripps DNA Array core for their assistance with the gene array experiment.

REFERENCES

1. Kang SS, McGavern DB. Lymphocytic choriomeningitis infection of the central nervous system. Front Biosci. 13; 2008:4529–4543.
2. Marker O, Nielsen MH, Diemer NH. The permeability of the blood-brain barrier in mice suffering from fatal lymphocytic choriomeningitis virus infection. Acta Neuropathol. 1984; 63:229–239. [PubMed: 6464679]
3. Camenga DL, Walker DH, Murphy FA. Anticonvulsant prolongation of survival in adult murine lymphocytic choriomeningitis. I. Drug treatment and virologic studies. J Neuropathol Exp Neurol. 1977; 36:9–20. [PubMed: 833620]
4. Fung-Leung WP, Kundig TM, Zinkernagel RM, Mak TW. Immune response against lymphocytic choriomeningitis virus infection in mice without CD8 expression. J Exp Med. 1991; 174:1425–1429. [PubMed: 1683893]
5. Bajenoff M, et al. Stromal cell networks regulate lymphocyte entry, migration, and territoriality in lymph nodes. Immunity. 2006; 25:989–1001. [PubMed: 17112751]
6. Bromley SK, Peterson DA, Gunn MD, Dustin ML. Cutting edge: hierarchy of chemokine receptor and TCR signals regulating T cell migration and proliferation. J Immunol. 2000; 165:15–19. [PubMed: 10861029]
7. Storm P, Bartholdy C, Sorensen MR, Christensen JP, Thomsen AR. Perforin-deficient CD8+ T cells mediate fatal lymphocytic choriomeningitis despite impaired cytokine production. J Virol. 2006; 80:1222–1230. [PubMed: 16414999]
8. Johnson ED, Monjan AA, Morse HC 3rd. Lack of B-cell participation in acute lymphocyte choriomeningitis disease of the central nervous system. Cell Immunol. 1978; 36:143–150. [PubMed: 305287]
9. Leist TP, Cobbold SP, Waldmann H, Aguet M, Zinkernagel RM. Functional analysis of T lymphocyte subsets in antiviral host defense. J Immunol. 1987; 138:2278–2281. [PubMed: 2435794]
10. Tepper RI, Coffman RL, Leder P. An eosinophil-dependent mechanism for the antitumor effect of interleukin-4. Science. 1992; 257:548–551. [PubMed: 1636093]
11. Kurihara T, Warr G, Loy J, Bravo R. Defects in macrophage recruitment and host defense in mice lacking the CCR2 chemokine receptor. J Exp Med. 1997; 186:1757–1762. [PubMed: 9362535]
12. Marchi N, et al. Seizure-promoting effect of blood-brain barrier disruption. Epilepsia. 2007; 48:732–742. [PubMed: 17319915]
13. Asensio VC, Campbell IL. Chemokine gene expression in the brains of mice with lymphocytic choriomeningitis. J Virol. 1997; 71:7832–7840. [PubMed: 9311871]
14. Kaech SM, Hemby S, Kersh E, Ahmed R. Molecular and functional profiling of memory CD8 T cell differentiation. Cell. 2002; 111:837–851. [PubMed: 12526810]
15. Wherry EJ, et al. Molecular signature of CD8+ T cell exhaustion during chronic viral infection. Immunity. 2007; 27:670–684. [PubMed: 17950003]
16. Andersen IH, Marker O, Thomsan AR. Breakdown of blood-brain barrier function in the murine lymphocytic choriomeningitis virus infection mediated by virus-specific CD8+ T cells. J Neuroimmunol. 1991; 31:155–163. [PubMed: 1704015]
17. Doherty PC, Allan JE, Lynch F, Ceredig R. Dissection of an inflammatory process induced by CD8+ T cells. Immunol Today. 1990; 11:55–59. [PubMed: 2110460]

18. Walker DH, Camenga DL, Whitfield S, Murphy FA. Anticonvulsant prolongation of survival in adult murine lymphocytic choriomeningitis. II. Ultrastructural observations of pathogenetic events. J Neuropathol Exp Neurol. 1977; 36:21–40. [PubMed: 188995]
19. Wedmore CV, Williams TJ. Control of vascular permeability by polymorphonuclear leukocytes in inflammation. Nature. 1981; 289:646–650. [PubMed: 7464931]
20. Bjork J, Arfors KE. Oxygen free radicals and leukotriene B4 induced increase in vascular leakage is mediated by polymorphonuclear leukocytes. Agents Actions Suppl. 1982; 11:63–72. [PubMed: 6295114]
21. Rosengren S, Ley K, Arfors KE. Dextran sulfate prevents LTB4-induced permeability increase, but not neutrophil emigration, in the hamster cheek pouch. Microvasc Res. 1989; 38:243–254. [PubMed: 2481803]
22. Hixenbaugh EA, et al. Stimulated neutrophils induce myosin light chain phosphorylation and isometric tension in endothelial cells. Am J Physiol. 1997; 273:H981–H988. [PubMed: 9277518]
23. Sekido N, et al. Prevention of lung reperfusion injury in rabbits by a monoclonal antibody against interleukin-8. Nature. 1993; 365:654–657. [PubMed: 8413628]
24. Herwald H, et al. M protein, a classical bacterial virulence determinant, forms complexes with fibrinogen that induce vascular leakage. Cell. 2004; 116:367–379. [PubMed: 15016372]
25. Tacke F, et al. Monocyte subsets differentially employ CCR2, CCR5, and CX3CR1 to accumulate within atherosclerotic plaques. J Clin Invest. 2007; 117:185–194. [PubMed: 17200718]
26. Maus U, et al. The role of CC chemokine receptor 2 in alveolar monocyte and neutrophil immigration in intact mice. Am J Respir Crit Care Med. 2002; 166:268–273. [PubMed: 12153956]
27. Ancuta P, Moses A, Gabuzda D. Transendothelial migration of CD16+ monocytes in response to fractalkine under constitutive and inflammatory conditions. Immunobiology. 2004; 209:11–20. [PubMed: 15481136]
28. Stamatovic SM, et al. Monocyte chemoattractant protein-1 regulation of blood-brain barrier permeability. J Cereb Blood Flow Metab. 2005; 25:593–606. [PubMed: 15689955]
29. Intlekofer AM, et al. Anomalous type 17 response to viral infection by CD8+ T cells lacking T-bet and eomesodermin. Science. 2008; 321:408–411. [PubMed: 18635804]
30. Beal AM, et al. Protein kinase Ctheta regulates stability of the peripheral adhesion ring junction and contributes to the sensitivity of target cell lysis by CTL. J Immunol. 2008; 181:4815–4824. [PubMed: 18802085]

METHODS REFERENCES

31. McGavern DB, Christen U, Oldstone MB. Molecular anatomy of antigen-specific CD8(+) T cell engagement and synapse formation in vivo. Nat Immunol. 2002; 3:918–925. [PubMed: 12352968]
32. Faust N, Varas F, Kelly LM, Heck S, Graf T. Insertion of enhanced green fluorescent protein into the lysozyme gene creates mice with green fluorescent granulocytes and macrophages. Blood. 2000; 96:719–726. [PubMed: 10887140]
33. Crozat K, et al. Jinx, an MCMV susceptibility phenotype caused by disruption of Unc13d: a mouse model of type 3 familial hemophagocytic lymphohistiocytosis. J Exp Med. 2007; 204:853–863. [PubMed: 17420270]
34. Revell PA, et al. Granzyme B and the downstream granzymes C and/or F are important for cytotoxic lymphocyte functions. J Immunol. 2005; 174:2124–2131. [PubMed: 15699143]
35. Lauterbach H, Zuniga EI, Truong P, Oldstone MB, McGavern DB. Adoptive immunotherapy induces CNS dendritic cell recruitment and antigen presentation during clearance of a persistent viral infection. J Exp Med. 2006; 203:1963–1975. Epub 2006 Jul 1917. [PubMed: 16847068]
36. Kim JV, Dustin ML. Innate response to focal necrotic injury inside the blood-brain barrier. J Immunol. 2006; 177:5269–5277. [PubMed: 17015712]

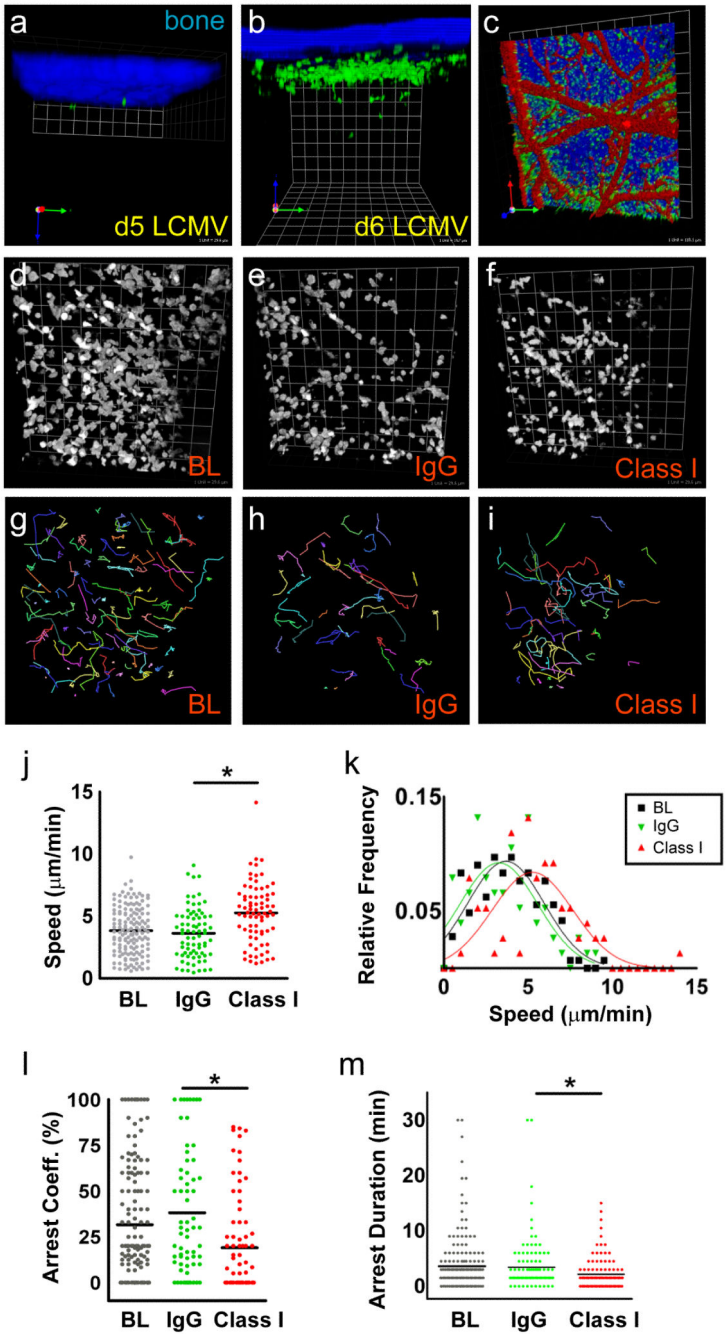

Figure 1. CTL localization and dynamics in the meninges of LCMV-infected mice

a,b, A representative 3D reconstruction of an intravital two-photon *z*-stack viewed through a thinned skull is shown for representative mice at day 5 (**a**) and day 6 (**b**) post-infection. Few GFP^+ P14 CTL (green) were observed in the meninges at day 5 post-infection. At day 6 post-infection GFP^+ P14 CTL were confined to 50 μm meningeal space between the undersurface of the skull bone (blue) and the pial surface. Very few CTL entered the parenchyma. (Grid scale = 19.7 μm) **c**, A representative 3D reconstruction shows that GFP^+ P14 CTL (green) localized preferentially along meningeal vasculature (red) at day 6. Skull

bone is blue. (Grid scale = 119 μm) **d–i**, Representative *xy* plane thinned skull images of GFP^+ P14 cells at day 6 post-infection (gray scale) (**d–f**) and corresponding 30 minute time lapse cell tracks (colored lines) (**g–i**) below each image are shown. (Representative *xz* planes images are shown in Supplementary Figure 1.) Note the highly dynamic motion of the CTL in the meningeal surface at baseline (BL) (**d, g**) and following injection of 10 μg/mL IgG isotype control (IgG) (**e, h**) or anti-H-$2D^b$ antibody (class I) (**f,i**). (Grid scale = 29.6 μm) **j–m,** Compared with baseline and IgG isotype control, class I inhibition induced a statistically significant (*$p < 0.0001$) change in average speed (**j**), arrest coefficient (**l**), and arrest duration (**m**) for GFP^+ P14 CTL. Primary velocity data shown in panel **j** are plotted as histograms using 5 μm/min bins and a Gaussian curve fit (**k**). See corresponding Movie 1 and Figure S1.

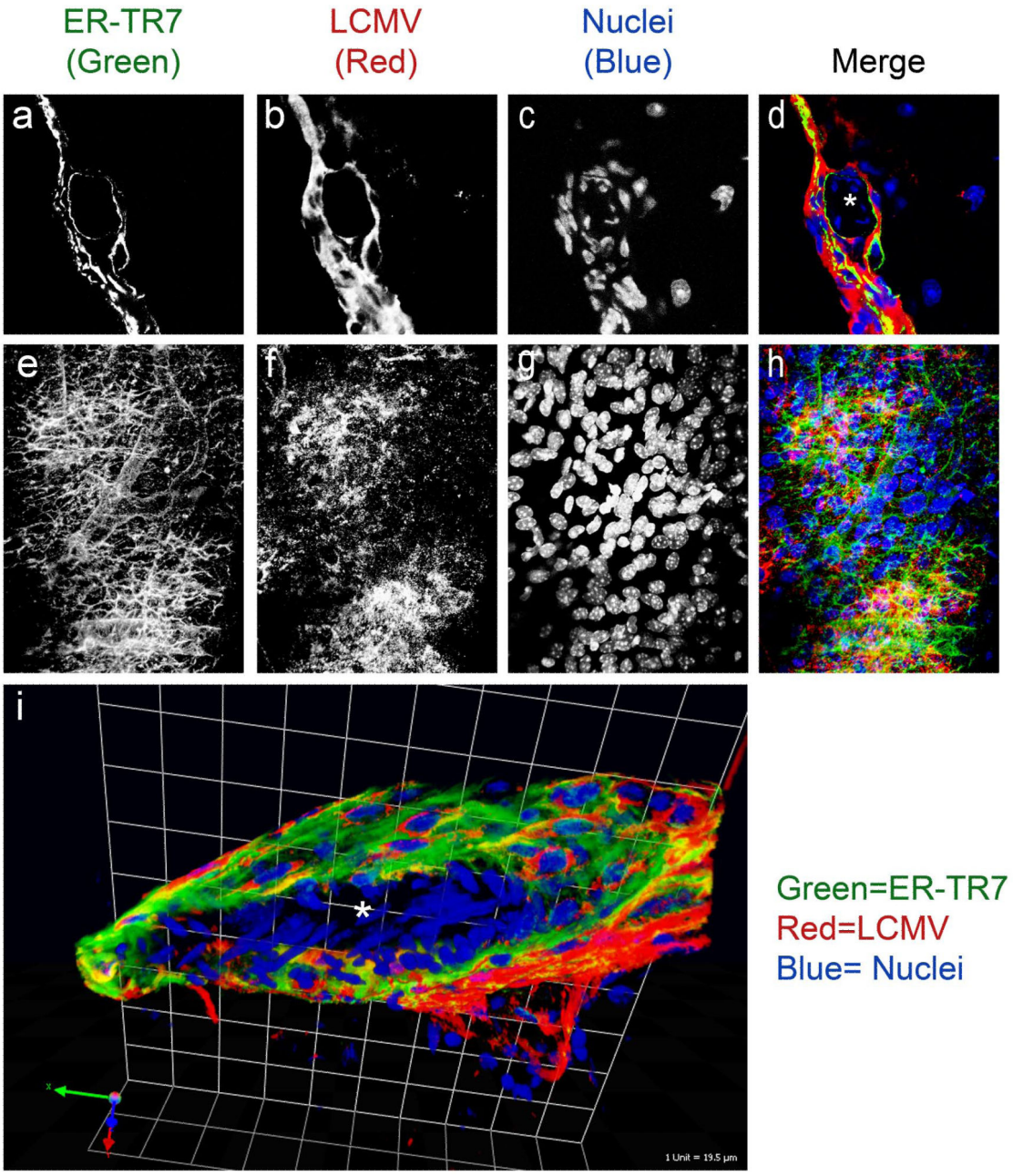

Figure 2. LCMV infection of ER-TR7+stromal cells in the meninges

a–h, A representative 2D image (**a–d**) and a maximal projection of a 3D *z*-stack (**e–h**) are shown for a mouse at day 6 post-infection. Both images were captured using a one-photon confocal microscope. Note the localization of LCMV (red) to ER-TR7^{+} fibroblast-like cells (green) that line the meninges and meningeal vasculature. A cross section of a meningeal blood vessel is denoted with a white asterisk in panel **d**. Panels **e–h** depict a top down view of a large meningeal blood vessel where the network of fibroblast processes are clearly visible and infected by LCMV. **i**, A 3D reconstruction of a meningeal blood vessel cross

section (center denoted with a white asterisk) is shown to illustrate the degree to which LCMV infects fibroblast-like cells that completely surround meningeal blood vessels. (Grid scale = 19.5 μm) Cell nuclei are shown in blue in all merged panels. See corresponding Movie 2 and Figure S3.

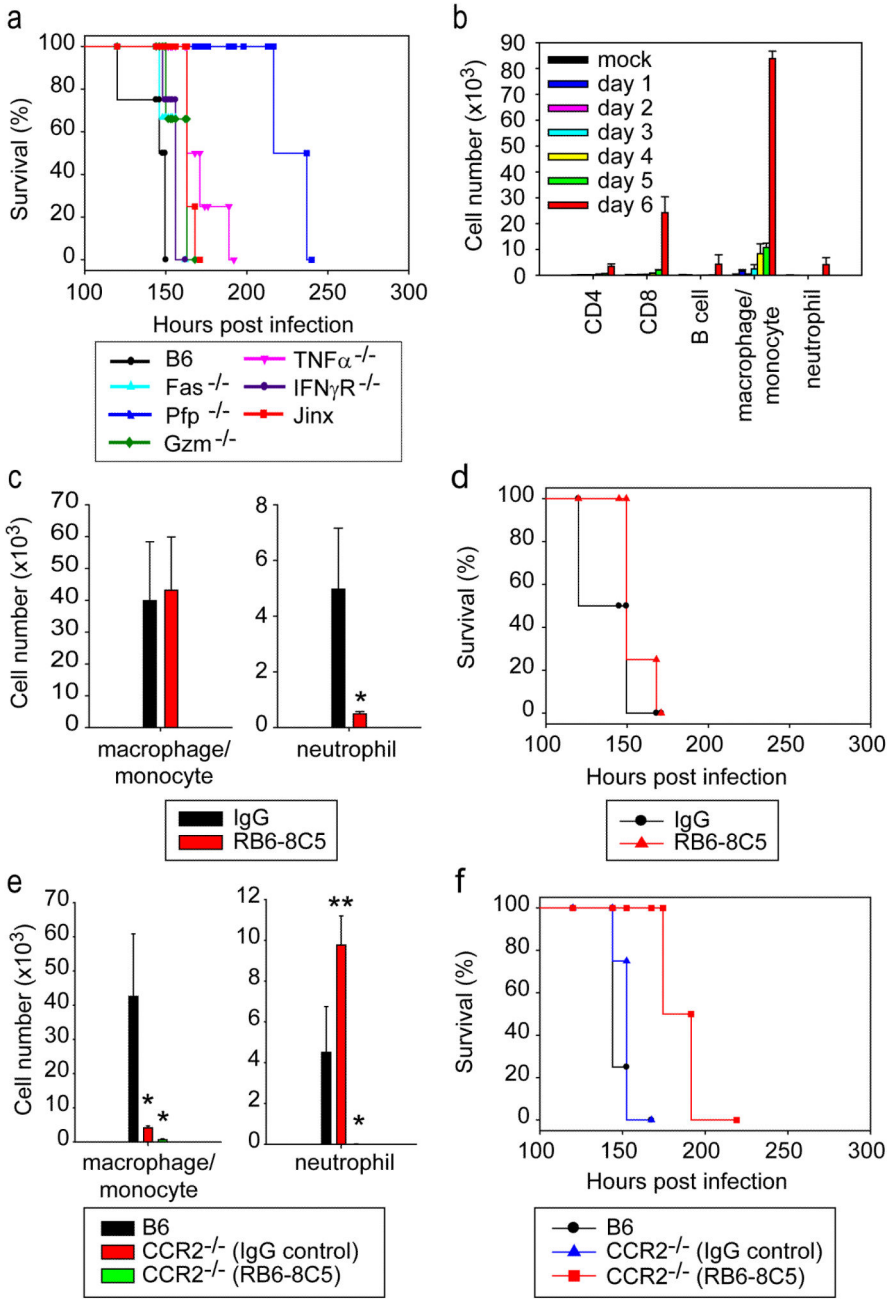

Figure 3. Analysis of mononuclear cell infiltrate and effector mechanisms during LCMVinduced meningitis

a, Survival was monitored in mice deficient in all major CTL effector pathways. Note that all infected knockout mice develop convulsive seizures and succumb to LCMV-induced meningitis. A slight extension (13 hrs, $p = 0.029$) in survival was observed in TNF-α knockout and *Jinx* mice. As reported previously, perforin deficient mice survived until day 9 ($p = 0.029$). **b,** The composition of the CNS mononuclear cell infiltrate was examined flow cytometrically at the denoted time points following LCMV infection. A massive influx of

CTL ($CD45^{+}Thy1.2^{+}CD8^{+}$) and peripheral monocytes ($CD45^{hi}Thy1.2^{-}CD11b^{+}Gr\text{-}1^{int}$) into the CNS was observed only at day 6 post-infection. Low numbers of neutrophils ($CD45^{int}Thy1.2^{+}CD11b^{+}Gr\text{-}1^{hi}$), B cells ($CD45^{+}Thy1.2^{+}CD19^{+}$), and CD4 T cells ($CD45^{+}Thy1.2^{+}CD4^{+}$) were also observed in the CNS at day 6 post-infection. See Figure S5 for examples of flow cytometric data. **c, d,** Injection of low dose anti-Gr-1 antibody (125 μg i.p. on day 4) achieved depletion of neutrophils from the CNS (**c**), but did not improve survival (**d**) when compared to control mice treated with rat IgG. **e, f,** CCR2 deficiency did not improve survival (**f**) following i.c. LCMV infection when compared to wild type B6 controls; however, flow cytometric studies revealed a compensatory increase in the number of CNS neutrophils (**e**) in CCR2 knockout mice at day 6. Survival was significantly extended in LCMV-infected CCR2 deficient mice that received high dose anti-Gr-1 antibody (**f**). The frequency of $CD45^{+}$ P14 cells was not significantly reduced following anti-Gr-1 treatment (data not shown). For all studies described above n=4 mice per group were used.

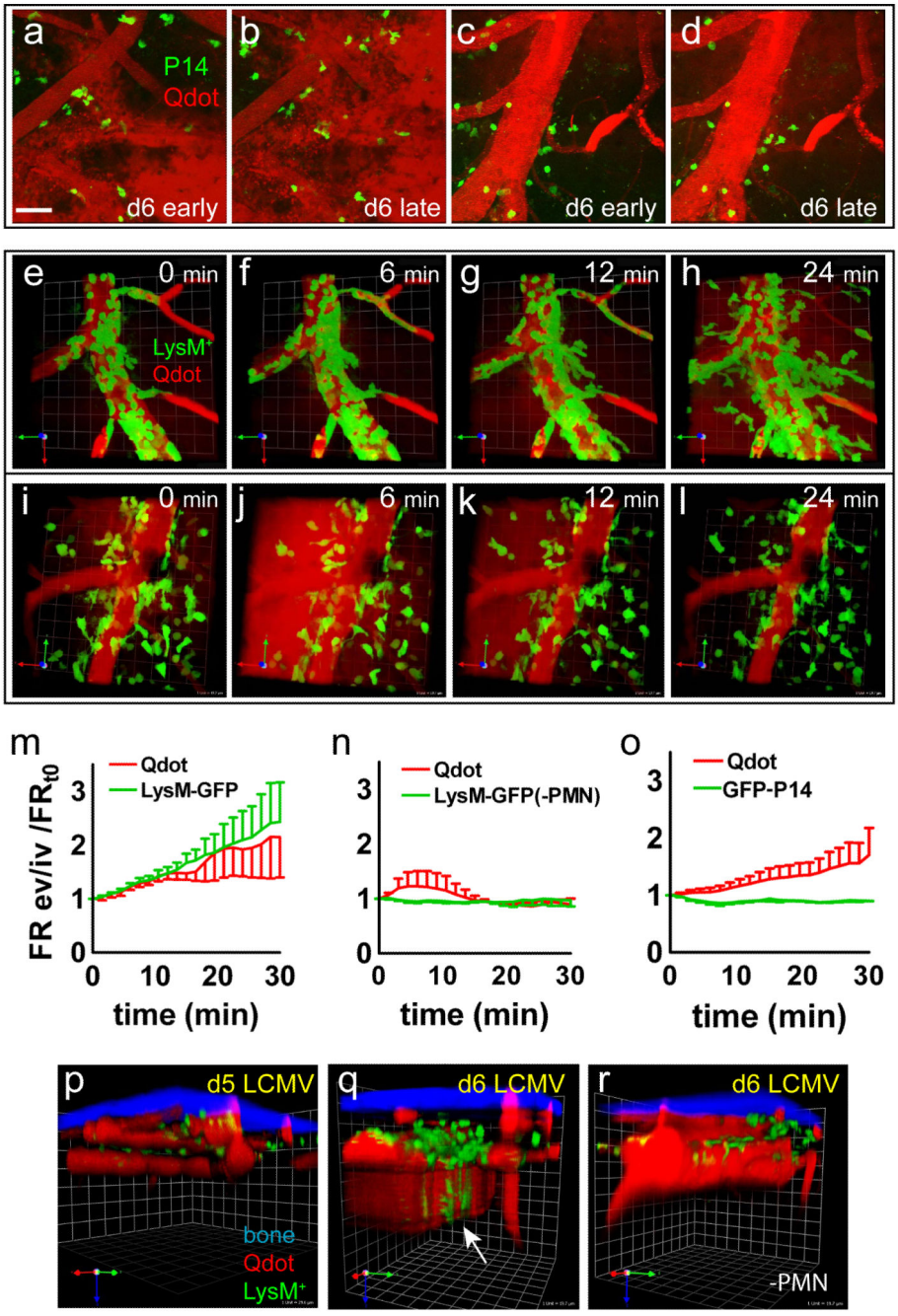

Figure 4. Recruitment of myelomonocytic cells into CNS and the relationship to meningeal vascular injury

a–d, Two representative two-photon images at early (t=0 min) (**a, c**) and late (t= 30 min) (**b, d**) points in the time lapse show the position of GFP$^+$ P14 CTL (green) in relation to meningeal vascular changes (red). GFP$^+$ CTL were typically found in perivascular regions. In panels **a–b** note the severe disruption of vascular integrity, as evidenced by the significant amount of extravascular quantum dot signal (red). Also note the ghost outlines of large cells near the ragged vessels that do not correspond to P14 CTL. In other areas P14 CTL

remained near perivascular areas that had preserved blood vessel integrity (**c, d**). (Scale = 50 μm) See corresponding Movie 3. **e–h**, A representative two-photon 30 minute time lapse sequence of vascular leakage of quantum dots (red) and extravasation of LysM-GFP$^+$ myelomonocytic cells (green) is shown for a symptomatic mouse at day 6 post-infection. Note that myelomonocytic cells roll and arrest inside the meningeal vessel before penetrating through the vascular wall and extravasating into the meningeal space. The extravasation of myelomonocytic cells is associated with severe vascular injury and quantum dot leakage. (Grid scale = 19.7 μm) See corresponding Movie 4. No similar extravasation events were observed in asymptomatic control mice at day 5 post-infection (data not shown). **i–l**, A representative 30 minute time lapse is shown for a symptomatic LysM-GFP depleted of neutrophils but not monocytes using low dose anti-Gr-1 antibody. Note that LysM-GFP$^+$ myelomonocytic cells (green) in the absence of neutrophils localize perivascularly and are associated with transient vascular leakage (red). (Scale = 25 μm) See corresponding Movie 5. **m–o,** The ratio of extravascular to intravascular GFP and quantum dot fluorescence signal was calculated at each frame, normalized to the baseline ratio, and plotted versus time. Data are represented as mean ± SEM. P14 CTL extravasation or positioning was not associated with quantum dot leakage (**o**). Leakage appeared to be associated with unlabeled ghost cells in CTL movies. Myelomonocytic cell extravastion correlated ($r = 0.99$; $p < 0.0001$) with sustained vascular leakage only in the presence of neutrophils (**m**). In neutrophil depleted LysM-GFP mice, perivascular myelomonocytic cells were associated with transient quantum dot leakage (**n**). **p–r,** Representative 3D reconstructions of two-photon *z*-stacks depicting skull bone (blue), quantum dot (red), and LysM-GFP$^+$ myelomonocytic cells (green) are shown for an asymptomatic mouse at day 5 (**p**), a symptomatic LysM-GFP mouse at day 6 (**q**), and a symptomatic LysM-GFP mouse at day 6 depleted of neutrophils (**r**). At day 5, vasculature showed smooth borders, no quantum dot (red) leakage, and few LysM-GFP$^+$ cells (green). In symptomatic mice at day 6, LysM-GFP$^+$ cells were mostly observed extravasating from meningeal vasculature with some cells accompanying the vascular leakage down into the parenchyma (white arrow). In mice depleted of neutrophils (PMN), LysM-GFP cells were observed in perivascular meningeal spaces. (Grid scale for panels **p–r** = 19.7 μm) See corresponding Movies 4, 5.